Atmospheric
Chemistry
and Physics
Discussions

Open Access

Energy transport, polar amplification, and ITCZ shifts in the GeoMIP G1 ensemble

Rick D. Russotto[1] and Thomas P. Ackerman[1,2]

[1]Department of Atmospheric Sciences, University of Washington, Seattle, Washington, USA
[2]Joint Institute for the Study of the Atmosphere and Ocean, University of Washington, Seattle, Washington, USA

Correspondence to: Rick D. Russotto (russotto@uw.edu)

Abstract.

The polar amplification of warming and the ability of the inter-tropical convergence zone (ITCZ) to shift to the north or south are two very important problems in climate science. Examining these behaviors in global climate models (GCMs) running solar geoengineering experiments is helpful not only for predicting the effects of solar geoengineering, but also for understanding

5   how these processes work under increased CO_2. Both polar amplification and ITCZ shifts are closely related to the meridional transport of moist static energy (MSE) by the atmosphere. This study examines changes in MSE transport in 10 fully coupled GCMs in Experiment G1 of the Geoengineering Model Intercomparison Project, in which the solar constant is reduced to compensate for abruptly quadrupled CO_2 concentrations. In G1, poleward MSE transport decreases relative to preindustrial conditions in all models, in contrast to the CMIP5 abrupt4xCO2 experiment, in which poleward MSE transport increases. Since

10 poleward energy transport decreases rather than increasing, and local feedbacks cannot change the sign of an initial temperature change, the residual polar amplification in the G1 experiment must be due to the different spatial patterns of the simultaneously imposed solar and CO_2 forcings. However, the reduction in poleward energy transport likely plays a role in limiting the polar warming in G1. An attribution study with a moist energy balance model shows that cloud feedbacks are the largest source of uncertainty regarding changes in poleward energy transport in mid-latitudes in G1, as well as for changes in cross-equatorial

15 energy transport, which are anticorrelated with ITCZ shifts.

1 Introduction

As solar geoengineering, or the artificial cooling of earth by reflecting sunlight, increasingly gains attention as part of a possible strategy to deal with the effects of climate change, two important issues are whether the polar amplification of CO_2-induced warming can be fully compensated for, and whether regional precipitation patterns will shift, exacerbating flooding in some

20 areas and drought in others. Polar amplification is the phenomenon in which the poles warm by more than the tropics when atmospheric CO_2 concentrations are increased. While the reasons for polar amplification are not yet completely understood, it has already been observed in the instrumental temperature record (*e.g.* Bekryaev et al., 2010) and is a robust behavior in climate models (*e.g.* Holland and Bitz, 2003). Since reflecting sunlight would affect Earth's radiation budget through different physical mechanisms from changes in CO_2 concentrations, it has been hypothesized that solar geoengineering may insufficiently cool

the polar regions. Early model simulations of solar geoengineering scenarios, involving a simultaneous CO_2 increase and solar constant decrease (Govindasamy and Caldeira, 2000; Govindasamy et al., 2003), found that most of the difference in warming between the poles and the tropics was, in fact, eliminated. However, these types of experiments still result in some warming at the poles and cooling in the tropics if the global mean temperature is held constant; we refer to this effect as "residual polar amplification".

Questions about shifts in regional precipitation under solar geoengineering are motivated by evidence from paleoclimate data and climate model studies that if one hemisphere is preferentially warmed, the intertropical convergence zone (ITCZ) shifts toward that hemisphere (*e.g.* Broccoli et al., 2006). Model studies have shown that such an effect could occur for changes in many different variables that affect the inter-hemispheric albedo contrast, such as high-latitude ice cover (Chiang and Bitz, 2005), mid-latitude forest extent (Swann et al., 2012), and tropospheric sulfate aerosol concentration (Hwang et al., 2013). In the context of solar geoengineering, Haywood et al. (2013) demonstrated that preferentially injecting reflective aerosols into one hemisphere shifts the ITCZ towards the other hemisphere, causing drought in some subtropical areas. Even for a hemispherically symmetric solar geoengineering deployment, ITCZ shifts might still occur, due to differing albedos and/or radiative feedbacks between hemispheres.

Both polar amplification and ITCZ shifts are closely related to the meridional transport of energy by the atmosphere. Much progress has been made understanding atmospheric energy transport in a changing climate through projects in which multiple global climate models (GCMs) are run for the same radiative forcing scenarios. Hwang and Frierson (2010) showed that poleward transport of atmospheric moist static energy (MSE) increases under increased CO_2 concentrations in Coupled Model Intercomparison Project, Phase 3 (CMIP3) models. They used a moist energy balance model (EBM) to attribute the change in MSE transport across $40°$ latitude to different forcing and feedback terms, and found that cloud feedbacks are responsible for most of the inter-model spread in this quantity. Hwang et al. (2011) found that poleward dry static energy (DSE) transport in mid-to-high latitudes decreases with warming due to the reduced equator-to-pole temperature gradient (since warming is amplified at the poles), but moisture transport increases due to the overall warming combined with the nonlinearity of the Clausius-Clapeyron equation and the increase in moisture transport is enough to lead to an increase in MSE transport overall. Frierson and Hwang (2012) found that shifts in the ITCZ with warming in the CMIP3 slab ocean ensemble are anticorrelated with changes in atmospheric energy transport across the equator, with cloud feedbacks again being the largest source of uncertainty.

The Geoengineering Model Intercomparison Project (GeoMIP) provides an opportunity to use similar methods to investigate how atmospheric energy transport may change under solar geoengineering conditions, which can help us understand the reasons for residual polar amplification and tropical precipitation shifts. We analyze the results of GeoMIP experiment G1 (Kravitz et al., 2011), in which the solar constant is reduced at the same time as the CO_2 concentration is quadrupled in order to keep the global mean temperature approximately at preindustrial levels. For comparison, we also examine two CMIP5 model runs: piControl, a preindustrial run, and abrupt4xCO2, in which CO_2 is quadrupled but the solar constant remains the same.

GeoMIP has yielded insights into how temperature and precipitation patterns may change under solar geoengineering. Kravitz et al. (2013a) found that residual polar amplification occurs in all models running the G1 experiment. Global mean

precipitation decreases in G1 because the reduction in solar radiative flux at the surface is primarily balanced by a reduction in evaporation (Kravitz et al., 2013b). The precipitation reduction is evident over monsoonal land regions, as well as in the global mean, and extreme precipitation events are reduced in G1, in contrast to an increase in abrupt4xCO2 (Tilmes et al., 2013).

Reducing the solar constant is an approximation of more realistic proposals for solar geoengineering, such as injecting aerosols into the stratosphere. One example of how the physics differs between these scenarios involves the magnitude of the reduction in global mean precipitation. Solar constant reduction experiments underestimate the precipitation reduction compared to model runs that increase the concentration of sulfate aerosols in the stratosphere (Niemeier et al., 2013; Ferraro and Griffiths, 2016). This is because sulfate aerosols absorb longwave radiation, which reduces the net atmospheric radiative cooling rate and therefore allows for less precipitation, since the latent heat release from precipitation formation must be balanced by net radiative cooling. (See, *e.g.*, Pendergrass and Hartmann (2014) for a discussion of the atmospheric energy constraints on global mean precipitation). Even with this caveat, the G1 experiment is useful because of its simplicity and because it eliminates confounding effects from global mean temperature changes.

We use the G1 experiment to investigate changes in meridional energy transport under solar geoengineering, the factors responsible for these changes, and the associated effects on tropical precipitation and polar amplification. Section 2 describes the energy and moisture transport changes that occur in the G1 and abrupt4xCO2 experiments. Section 3 attributes these energy transport changes to different forcing and feedback terms, using the moist energy balance model (EBM) of Hwang and Frierson (2010). Conclusions are provided in Section 4.

2   Energy and moisture transport changes

Using the top of atmosphere (TOA) and surface energy and moisture fluxes from the GeoMIP GCM experiments, we calculate changes in the meridional transport of MSE by the atmosphere. By subtracting the MSE transport in piControl from that in G1, we can understand how the combined CO_2 increase and solar constant decrease affect MSE transport, or, in other words, how well solar reductions can restore preindustrial patterns of atmospheric energy transport. For comparison, we also examine how the CO_2 increase alone affects MSE transport by subtracting the MSE transport in piControl from that in abrupt4xCO2. Following Kravitz et al. (2013a) and other papers analyzing GeoMIP results, we use the average of years 11-50 of the G1 and abrupt4xCO2 experiments in order to exclude the rapid changes that occur during the first few years. For piControl, we average over the first 40 years of model output provided by the modeling groups. (The period analyzed does not include any model spin-up period.)

We calculate the energy flux into the atmosphere from the GCM output as the sum of terms on the right-hand side of the following energy budget equation:

$$\nabla \cdot F_M = R_{\text{net,TOA}}^{\downarrow} + R_{\text{net,surface}}^{\uparrow} + \text{SH} + \text{LH} \tag{1}$$

where F_M is the vertically integrated moist static energy flux, $R_{\text{net,TOA}}^{\downarrow}$ is the net downward radiative flux at the top of the atmosphere, $R_{\text{net,surface}}^{\uparrow}$ is the net upward radiative flux at the surface, SH is the net upward surface sensible heat flux, and LH

Table 1. Models included in this study, with references, institutions, and solar constant reduction in the G1 experiment.

Model	Reference	Institution	S_0 reduction in G1
CanESM-2	Arora et al. (2011)	Canadian Centre for Climate Modeling and Analysis	4.0%
CCSM4	Gent et al. (2011)	National Center for Atmospheric Research	4.1%
CESM-CAM5.1-FV	Hurrell et al. (2013)	National Center for Atmospheric Research	4.7%
CSIRO-Mk3L-1-2*	Phipps et al. (2011)	Commonwealth Scientific and Industrial Research Organization/	3.2%
		Bureau of Meteorology	
GISS-E2-R*	Schmidt et al. (2014)	NASA Goddard Institute for Space Studies	4.5%
HadGEM2-ES	Collins et al. (2011)	Met Office Hadley Centre	3.9%
IPSL-CM5A-LR	Dufresne et al. (2013)	Institut Pierre Simon Laplace	3.5%
MIROC-ESM	Watanabe et al. (2011)	Atmosphere and Ocean Research Institute (The University of Tokyo),	5.0%
		National Institute for Environmental Studies,	
		and Japan Agency for Marine-Earth Science and Technology	
MPI-ESM-LR	Giorgetta et al. (2013)	Max Planck Institute for Meteorology	4.7%
NorESM1	Bentsen et al. (2013)	Bjerknes Centre for Climate Research,	4.0%
		Norwegian Meteorological Institute	

* These models are excluded from the second part of this study (the EBM analysis) because the necessary output fields were not archived.

is the net upward surface latent heat flux. Since the net energy flux into the atmospheric column must be balanced by energy transport out of the column, we can calculate the northward atmospheric moist static energy transport as a function of latitude by integrating $\nabla \cdot F_M$, first zonally and then cumulatively northward from the south pole. It is also useful to decompose the MSE transport into latent energy (moisture) transport and dry static energy (DSE) transport, in order to identify how moisture changes affect the total energy transport changes. We calculate the latent energy transport from the latent heat flux and precipitation GCM output by integrating the following equation zonally and meridionally:

$$\nabla \cdot F_L = \text{LH} - L_v P \tag{2}$$

where L_v is the latent heat of vaporization of water and P is precipitation. We calculate the DSE transport by subtracting the latent energy transport from the MSE transport.

Table 1 lists the GeoMIP models included in this analysis. Three of the original 13 GeoMIP models are excluded: BNU-ESM, because it did not adequately restore the global mean temperature in G1 and because the surface upwelling LW radiation is less than the downwelling LW, an unphysical result; EC-Earth, because the precipitation output file was corrupted; and HadCM3, because many of the output fields required for this study are no longer available. Methodological details of these calculations are described in Appendix A.
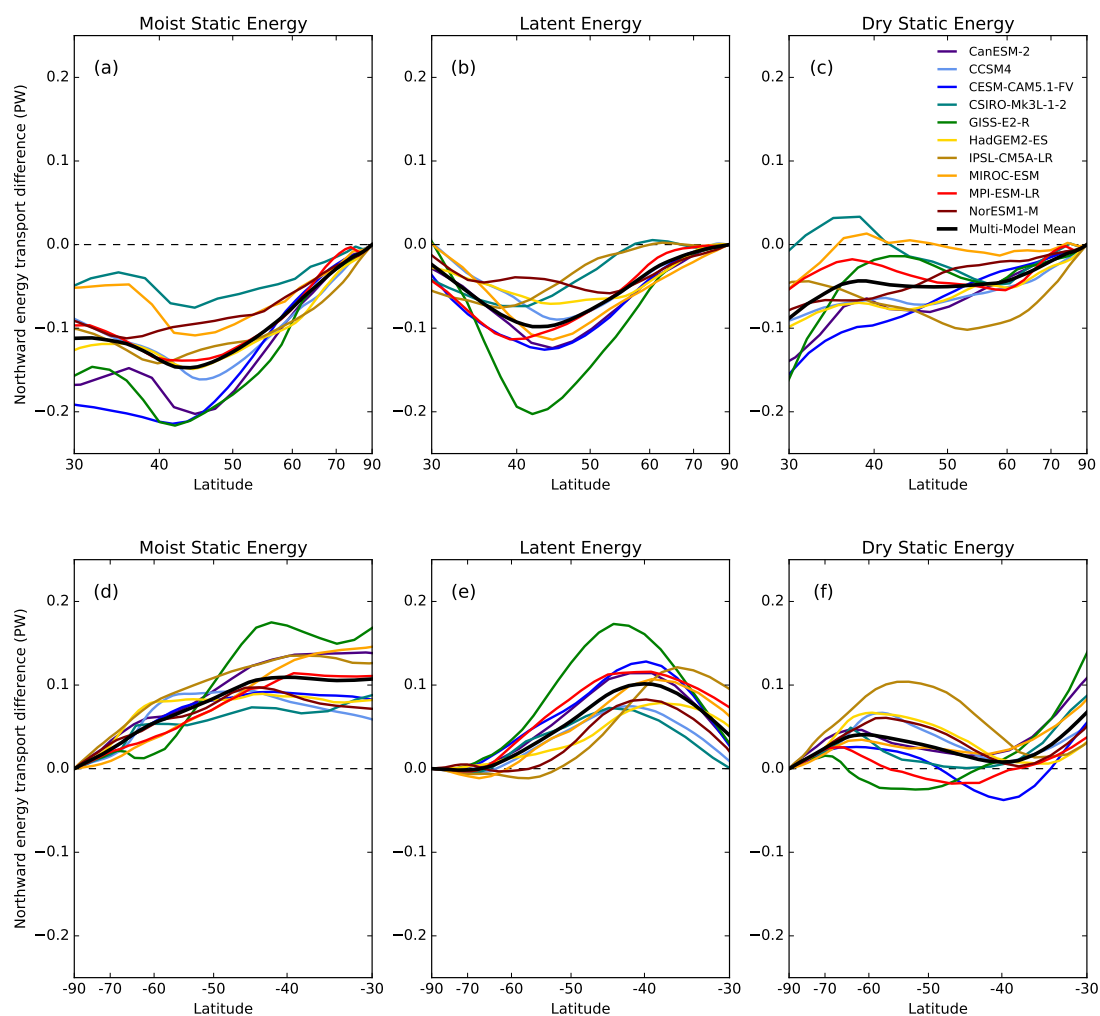
Figure 1. Northward energy transport (PW) for G1 minus piControl, poleward of 30° N (a-c) and 30° S (d-f), for total moist static energy transport (a, d), latent energy transport (b, e), and dry static energy transport (c, f), in the GeoMIP models and the multi-model mean.

2.1 Poleward transport in mid-latitudes

Changes in the zonal mean northward MSE, latent energy and dry static energy (DSE) transport for G1 minus piControl are shown in Figure 1. Poleward MSE transport in mid-latitudes is reduced under G1 in all 10 models and, when decomposed into the latent and DSE components, both of these terms are reduced as well. Figure 2 shows the same calculations for abrupt4xCO2 minus piControl. In this case, poleward DSE transport decreases but moisture transport increases by more than enough to
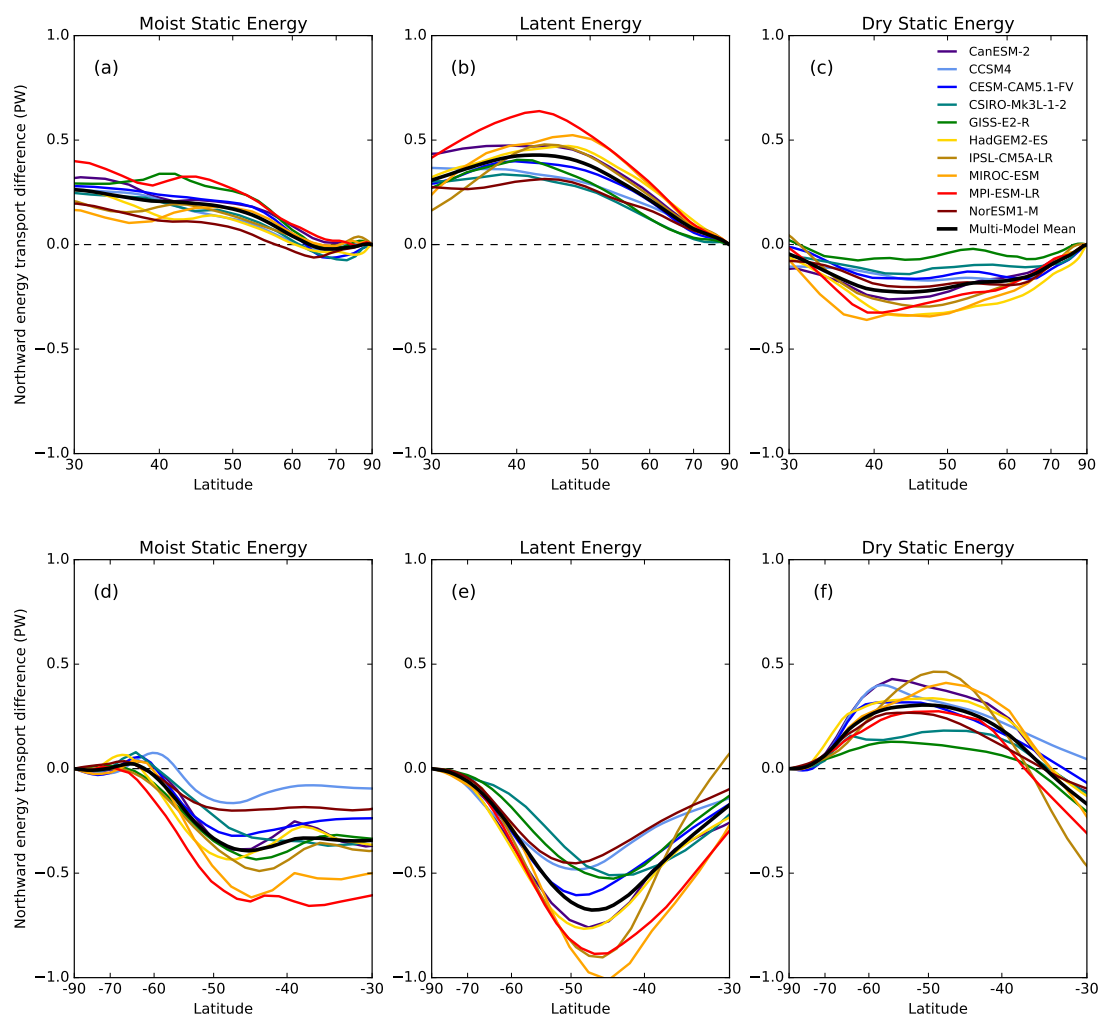
5

Figure 2. As in Figure 1 but for abrupt4xCO2 minus piControl.

compensate, leading to an increase in total MSE transport. This corroborates the result seen by Held and Soden (2006) and Hwang et al. (2011) in CMIP3 global warming scenarios.

To understand why the energy transport changes are different for global warming and geoengineering conditions, we look at zonal mean changes in temperature and saturation vapor pressure. Figures 3a,b show the zonal mean temperature change in G1 and abrupt4xCO2 relative to preindustrial. (These are also plotted in Figure 1 of Kravitz et al. (2013a), but our plots include only the models analyzed here and, for G1, we use a smaller y-axis range to show more detail.) In G1, the tropics are cooled while the poles are warmed (Figure 3a). There is warming everywhere in abrupt4xCO2 but more so in the polar regions,
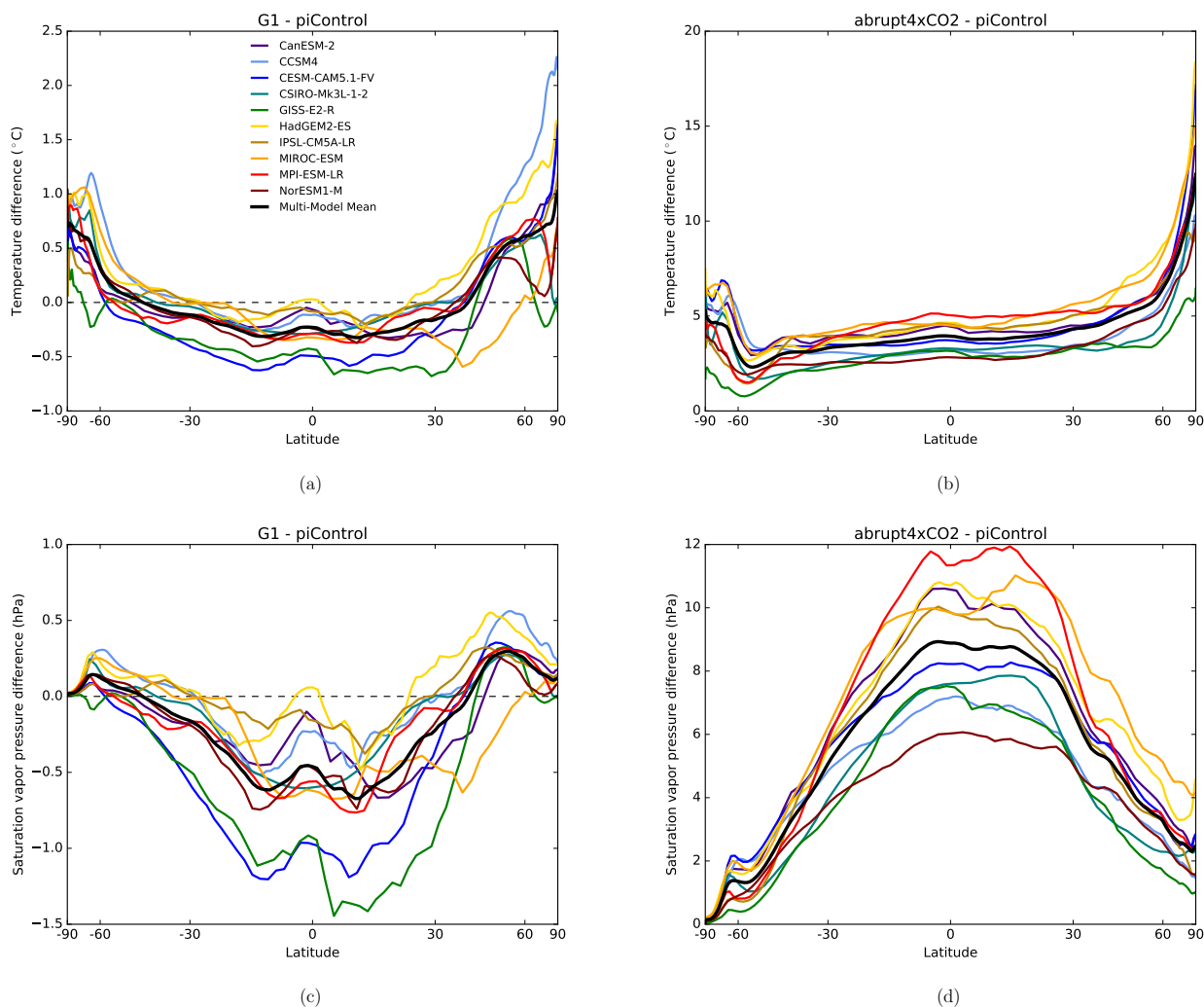
Figure 3. Zonal mean temperature changes relative to piControl for G1 (a) and abrupt4xCO2 (b), and analogous zonal mean saturation vapor pressure changes (c,d), in GeoMIP models and multi-model mean.

especially the Arctic (Figure 3b). In both cases, this pattern of temperature change results in a weakening of the equator-to-pole temperature gradient and reduces the poleward transport of dry static energy.

The mechanism for the difference in moisture transport is apparent from changes in saturation vapor pressure, e_s, which we calculate using an approximate form of the Clausius-Clapeyron equation (*e.g.* Hartmann, 2016, eq. 1.11):

$$e_s = 6.11 \exp \left\{ \frac{L_v}{R_v} \left(\frac{1}{273} - \frac{1}{T} \right) \right\} \tag{3}$$

5

where L_v is the latent heat of vaporization of water, R_v is the gas constant for water vapor, and T is the temperature in K. In abrupt4xCO2 (Figure 3d), e_s increases more in the tropics than it does near the poles because e_s is approximately exponential with respect to temperature. A slight warming in the tropics leads to a larger increase in e_s because the tropics were initially warmer than the poles. In G1, however (Figure 3c), the tropics cool and the poles warm, so saturation vapor

5   pressure, like temperature, decreases in the tropics and increases (to a lesser extent) at high latitudes relative to piControl. Assuming the moisture content in the atmosphere scales with Clausius-Clapeyron, and the meridional winds are roughly the same, poleward moisture transport increases in abrupt4xCO2 and decreases in G1 because the equator-to-pole moisture gradient has strengthened in abrupt4xCO2 and weakened in G1.

In G1, poleward MSE transport decreases, but the poles are still warmed relative to the tropics. This implies that the residual
10   polar amplification in G1 must be due to the differing spatial patterns of the opposing solar and CO_2 forcings, with the solar forcing being greater in absolute magnitude in the tropics, where there is more sunlight to reduce. Local radiative feedbacks such as the ice-albedo feedback cannot be responsible for the residual polar amplification because these can only amplify or dampen a temperature change, but cannot reverse its sign. This leaves the differing spatial patterns of the forcings as the only possible explanation.

15   The decrease in poleward MSE transport likely diminishes the polar warming in G1, relative to what would happen if forcings and feedbacks were allowed to operate locally but energy transport was fixed at piControl levels. It would be a useful avenue for future research to quantify the effect of reduced energy transport, as well as local feedbacks, on the polar warming in G1, similar to the study of Arctic amplification under global warming by Pithan and Mauritsen (2014). The reduction in poleward moisture transport may help explain the reduction in mid-latitude precipitation seen in Tilmes et al. (2013); quantifying this
20   effect would also be a useful research direction.

2.2   Cross-equatorial energy transport and ITCZ shifts

Figure 4a shows the relationship between shifts in the ITCZ in G1 relative to piControl and changes in the transport of moist static energy across the equator. We define the position of the ITCZ as the latitude where half of the zonally integrated rainfall between 15°S and 15°N lies to the south and half lies to the north, following Hwang and Frierson (2010). In the multi-model
25   mean, the ITCZ shifts northward by 0.14 degrees, but there is significant inter-model spread, ranging from -0.33 to 0.89 degrees. These shifts are moderately anticorrelated with the change in cross-equatorial energy transport (correlation coefficient $r = -0.768$). Anticorrelation between these quantities is consistent with previous work (e.g. Frierson and Hwang, 2012; Hwang et al., 2013), and is expected because the Hadley cell transports energy primarily in its upper branch but moisture primarily in its lower branch. For ITCZ shifts in abrupt4xCO2, however, there is no correlation ($r = 0.071$; not shown). This may be
30   due to changes in ocean heat storage and transport that occur following an abrupt quadrupling of CO_2, which creates a large TOA energy imbalance. The G1 experiment was designed to keep the top of atmosphere in approximate energy balance, which limits changes in energy storage by the ocean.

Figure 4b shows the ITCZ shifts in G1 plotted against the warming of the northern hemisphere relative to the southern hemisphere in the same experiment. This is similar to Figure 7 of Smyth et al. (2017), but for the specific set of models
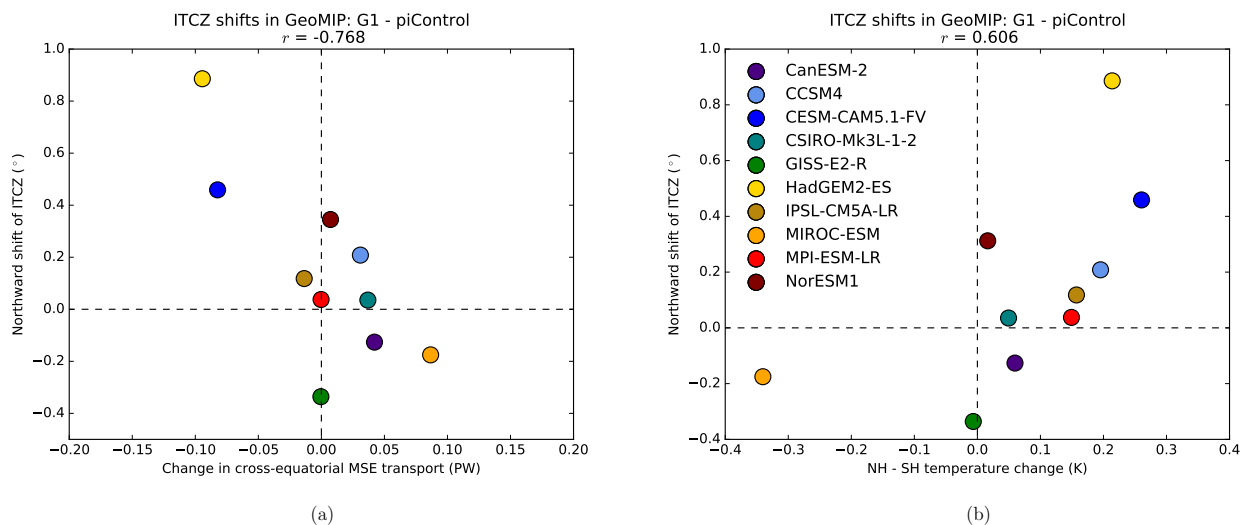
Figure 4. Shift in the ITCZ in GeoMIP models for G1 minus piControl, plotted against change in northward MSE transport across the equator (a) and northern hemisphere mean surface temperature change minus southern hemisphere mean temperature change (b). The quantity r is the correlation coefficient.

included in this study. Here, there is a positive correlation ($r = 0.606$), slightly weaker than that for cross-equatorial MSE transport. This corresponds to the idea that the ITCZ "shifts toward the warmed hemisphere". It implies that solar reductions applied equally in both hemispheres could still cause regional shifts in precipitation based on factors like the base state albedo and local radiative feedbacks that might warm one hemisphere relative to the other. This, along with reductions in the seasonal

5 ITCZ migration due to preferential cooling of the summer hemisphere, is discussed elsewhere (Smyth et al., 2017). Our focus here is on the reasons for the inter-model spread in the ITCZ shifts. These are more easily diagnosed using energy balance model attribution experiments aimed at understanding the causes for the changes in cross-equatorial energy flux.

3 Attribution of changes using a moist EBM

In order to investigate the causes of robust changes in meridional energy transport in the G1 experiment and the largest sources

10 of inter-model spread, we ran attribution experiments in which we perturbed different forcing and feedback terms one at a time. These experiments involved the moist energy balance model (EBM) first used by Hwang and Frierson (2010). We used the GCM output to calculate the magnitude of various forcings and feedbacks, including the greenhouse and solar forcings and cloud, surface albedo and non-cloud atmosphere feedbacks, and we used the EBM to understand how atmospheric energy transport would respond to each forcing or feedback in isolation. The advantage of using a moist EBM over directly integrating

15 the energy fluxes associated with each forcing or feedback is that it allows for a coupled response between the energy transport, local temperature, and longwave radiative cooling.

Atmospheric
Chemistry
and Physics
Discussions

Table 2. Summary of attribution experiments run with moist energy balance model.

Name	Effects considered	OLR fit from
APRPcloud	SW radiative response at TOA due to cloud changes	piControl
APRPnoncloud	SW radiative response at TOA due to non-cloud atmosphere changes	piControl
APRPsurface	SW radiative response at TOA due to surface albedo changes	piControl
solarForcing	solar constant change (for G1), or nonlinear SW feedbacks (for abrupt4xCO2)	piControl
surfaceFlux	net SW, LW, sensible and latent heat flux changes at surface; *i.e.* surface energy storage	piControl
LWCRE	difference in net TOA LW radiation between clear-sky and all-sky conditions	piControl
greenhouse	enhanced greenhouse effect	G1 or abrupt4xCO2
all_G1	sum of effects listed in first 7 rows	G1
all_4xCO2	sum of effects listed in first 7 rows	abrupt4xCO2

The "OLR fit" refers to the fitting of coefficients for a linearized greenhouse effect based on surface air temperature and clear-sky OLR output from the GCMs; shown in the table is which GCM experiment these fits were drawn from. Table 4 shows the actual fit coefficients.

The EBM takes as input the zonal mean surface and TOA energy fluxes and the LW cloud radiative effect from each GCM, and calculates the outgoing longwave radiation (OLR) as a function of surface temperature based on a linear fit of the clear-sky OLR and surface temperature output from each GCM. Net vertical energy flux convergences at each latitude are balanced by meridional diffusion of MSE. We obtained a meridional energy transport estimate from the EBM by meridionally integrating this diffusion term. Appendix B describes the methods for these experiments in more detail.

3.1 Comparison of EBM and GCM-derived energy transport

In order to be helpful in understanding the causes of the GCM behaviors, the EBM needs to predict changes in GCM-derived energy fluxes reasonably well when all forcing and feedback terms are considered. Figure 5 shows the meridional MSE transport across specific latitudes calculated by the EBM versus the same quantities diagnosed directly from the output of each GCM, for cross-equatorial transport in G1 minus piControl (Figure 5a), for poleward transport across 40°N in G1 minus piControl (Figure 5b), and for the same comparison in abrupt4xCO2 minus piControl(Figure 5c). There are generally strong correlations in each of these cases. Cross-equatorial energy transport changes in abrupt4xCO2 minus piControl are not examined because these did not correlate well with ITCZ shifts. Note that the cross-equatorial energy transport appears to change more easily in the GCMs than in the EBM, and the intercept is nonzero in Figure 5c. With these cautions in mind regarding the exact magnitude of the changes, the EBM predicts changes in GCM-derived energy fluxes well enough to proceed to the attribution experiments.

3.2 Attribution of cross-equatorial energy transport changes

The attribution experiments are summarized in Table 2. Two experiments, "all_G1" and "all_4xCO2", consider all of the forcing and feedback terms for the two perturbation climates. There are three experiments that perturb shortwave feedbacks,
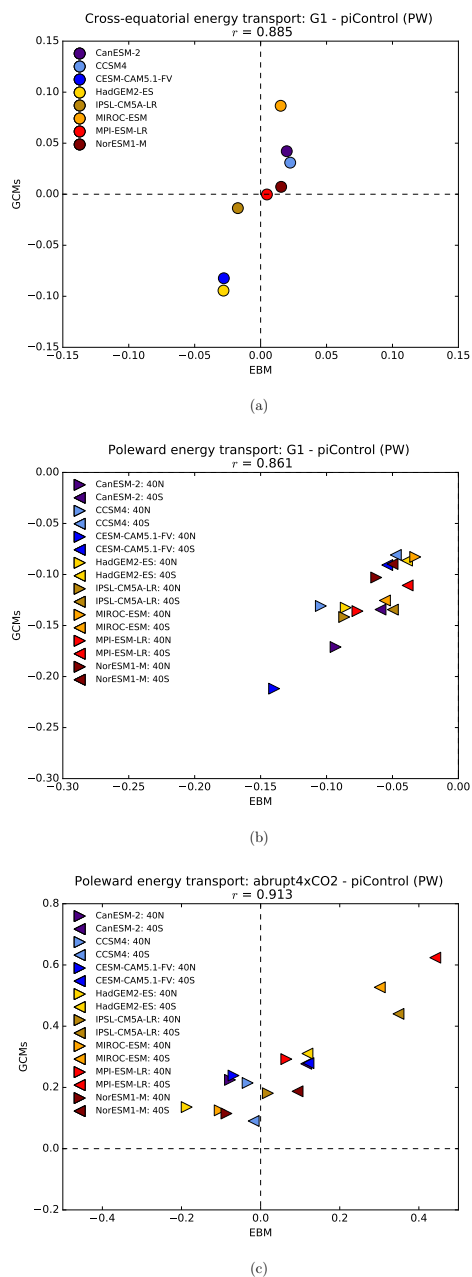
Figure 5. Meridional energy transport changes calculated by moist EBM (x-axis) versus those diagnosed from the GCM output (y-axis). (a): northward energy transport across the equator, for G1 minus piControl; (b): poleward energy transport changes across $40°$ N and S, for G1 minus piControl; (c): as in (b) but for abrupt4xCO2 minus piControl.
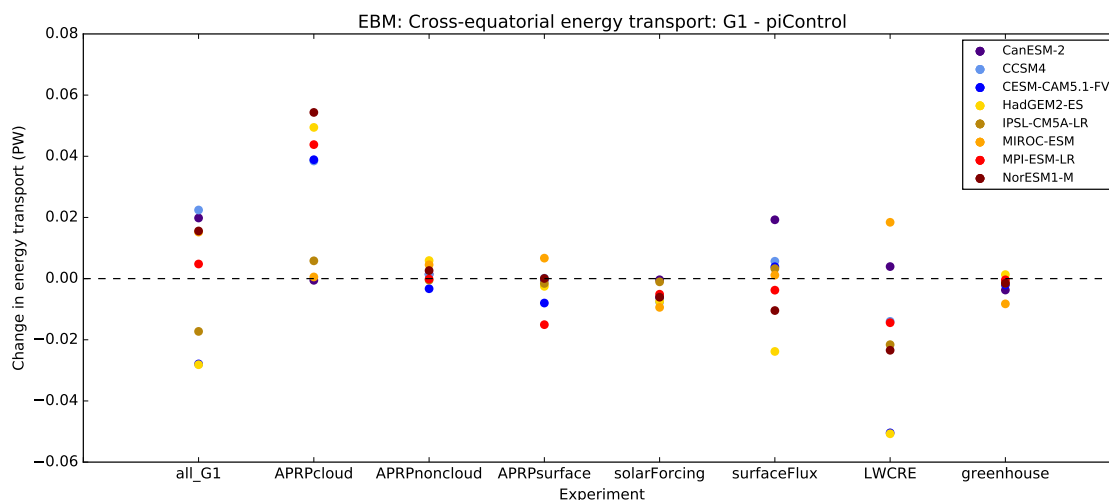
Figure 6. Changes in cross-equatorial energy transport calculated by moist EBM for G1 minus piControl in various attribution experiments.

based on the Approximate Partial Radiation Perturbation (APRP) method (Taylor et al., 2007). APRP uses a single-layer radiative transfer model to estimate the TOA radiative response to changes in clouds, non-cloud atmospheric scattering and absorption, and surface albedo, based on monthly mean GCM cloud fraction output and SW radiative flux output at the surface and TOA. We refer to our SW feedback attribution experiments as the "APRPcloud", "APRPnoncloud", and "APRPsurface"

5   experiments, which consider cloud, non-cloud atmosphere, and surface albedo feedbacks, respectively. The "solarForcing" experiment considers the change in insolation at the TOA due to the solar constant change. The "surfaceFlux" experiment considers the change in the net downward energy flux at the surface, which represents energy storage and transport by the ocean. The "LWCRE" experiment considers changes in the LW cloud radiative effect, or the difference between clear-sky and all-sky net TOA LW fluxes. Finally, the "greenhouse" experiment considers the enhanced clear-sky greenhouse effect, which

10   includes the CO_2 forcing and the water vapor, Planck and lapse rate feedbacks. The calculations of the input terms for the EBM for each experiment are described in more detail in Appendix B.

   Figure 6 shows the changes in northward energy transport across the equator for G1 minus piControl in each of the experiments listed in Table 2. The "all_G1" results are the same as those plotted on the x-axis on Figure 5a and show that there is considerable inter-model spread in the value of the cross-equatorial energy transport changes. None of the experiments shown

15   in Figure 6 moves cross-equatorial energy transport in the same direction in all 8 models (although the APRPcloud experiment comes close), so we cannot say with much confidence that any one forcing or feedback is likely to push the ITCZ one way or the other under a solar geoengineering scenario. However, it is useful to examine the inter-model spread in each experiment in order to determine which terms cause the most uncertainty in response of the ITCZ to solar geoengineering.

   The two attribution experiments with the largest inter-model spread are the APRPcloud and LWCRE experiments, which

20   correspond to SW and LW cloud feedbacks. This indicates that changes in clouds are the largest source of uncertainty regarding

how cross-equatorial energy transport and, therefore, the ITCZ would respond to a hemispherically symmetric solar geoengineering scenario. This is similar to the finding of Frierson and Hwang (2012) that cloud feedbacks are the largest source of uncertainty for cross-equatorial energy transport changes in slab ocean simulations of CO_2-induced warming.

The experiment with the next-largest inter-model spread is surfaceFlux, indicating that the hemispheric asymmetry of the
5 ocean heat uptake response to the combined solar and CO_2 forcings differs between the models. Solar forcing and surface albedo changes have smaller effects on cross-equatorial energy transport. The enhanced greenhouse effect, non-cloud atmospheric SW feedbacks, and solar forcing have the smallest effects on cross-equatorial energy transport. The impact of the solar forcing term depends on the base state surface and atmospheric albedo, because a spatially uniform solar constant reduction will have different effects on net TOA insolation depending on what fraction of the solar radiation would have otherwise been
10 reflected back to space had it not been reduced. Haywood et al. (2016) showed that tropical precipitation in the HadGEM2-ES is highly sensitive to the difference in the mean albedo between the hemispheres, but the small inter-model spread in the solarForcing experiment in Figure 6 suggests that the base state inter-hemispheric albedo difference is not the main source of inter-model spread in the ITCZ response to solar geoengineering.

3.3 Attribution of poleward energy transport changes
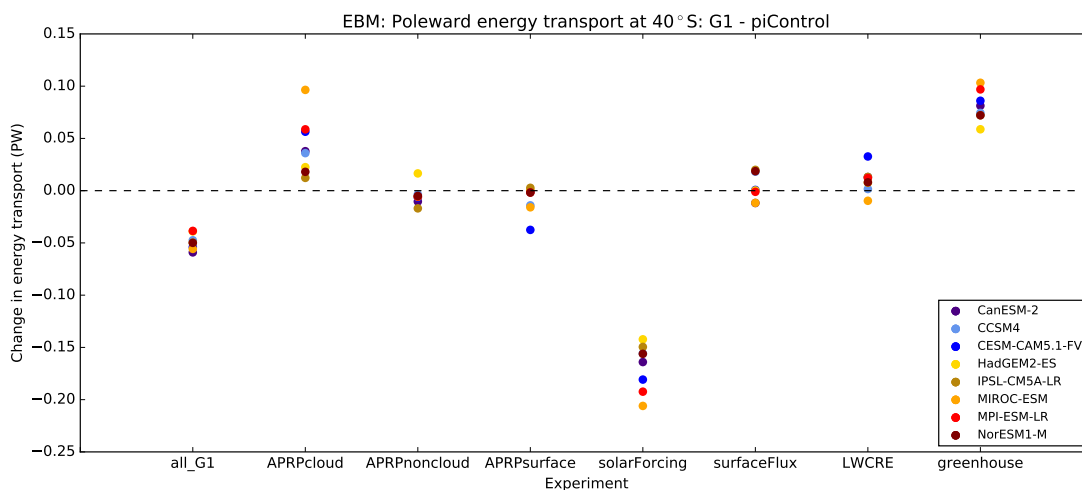
15 ### 3.3.1 G1 minus piControl

Figure 7 shows the results of the same attribution experiments shown in Figure 6, but for poleward energy transport at 40° N (Figure 7a) and 40° S (Figure 7b). In the all_G1 experiment, poleward energy transport decreases at this latitude in both hemispheres. Poleward energy transport decreases in the solarForcing experiment for each model, and increases in the greenhouse experiment, but not by enough to compensate. The increase in poleward transport in the greenhouse experiment can be
20 understood in terms of the increasing moisture transport argument discussed in Section 2 for the abrupt4xCO2 experiment. The radiative forcing is roughly spatially uniform, but atmospheric moisture increases more in the tropics than at the poles because the atmosphere was warmer in the tropics to begin with. The reduction in tropical moisture in the solarForcing case is greater than the increase in the greenhouse case because there is more sunlight to reduce in the tropics, causing a greater radiative perturbation there for solar reductions than for greenhouse gas increases.

25 None of the various feedback experiments has a consistent effect on the sign of the change of poleward energy transport in both hemispheres, but the feedback terms appear to rearrange the models in the all_G1 experiment, and contribute to the inter-model spread, with SW cloud feedbacks being the largest contributor. Models with a greater negative change in the solarForcing experiment also tend to have a greater positive change in the greenhouse experiment, and the compensation between these effects tends to reduce the inter-model spread. This implies that the remaining inter-model spread comes from
30 the feedback terms. The lack of a reduction in poleward energy transport associated with the surfaceFlux experiment rules out changes in ocean heat transport as a reason for the reduction in poleward energy transport. The fact that the solar forcing is the only term contributing to the reduction of poleward energy transport in G1 in all models implies that the imperfect compensation between SW and LW forcings, not local feedbacks, causes this reduction.
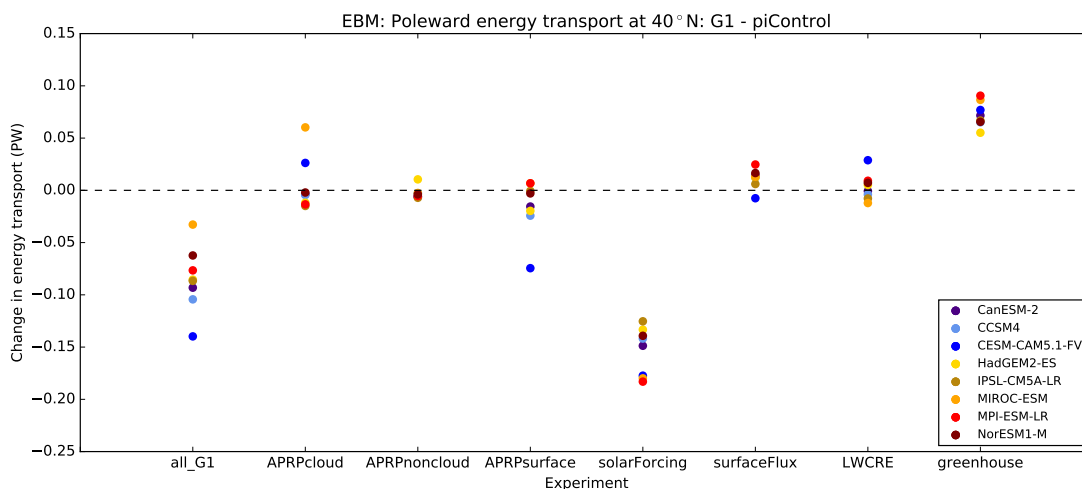
(a)

(b)

Figure 7. As in Figure 6 but for changes in poleward atmospheric energy transport across 40° N (a) and 40° S (b), for G1 minus piControl.

3.3.2 abrupt4xCO2 minus piControl

Figure 8 is the equivalent of Figure 7, but for abrupt4xCO2 minus piControl. For abrupt4xCO2, the greenhouse attribution experiment results in an increase in poleward energy transport, similar to the same experiment for G1. SW cloud feedbacks (APRPcloud experiment) are the largest contributor to the inter-model spread. Surface albedo feedbacks (APRPsurface) also contribute to the inter-model spread, but generally reduce poleward energy transport. (The increase in moisture due to tropical

5

Atmospheric
Chemistry
and Physics
Discussions
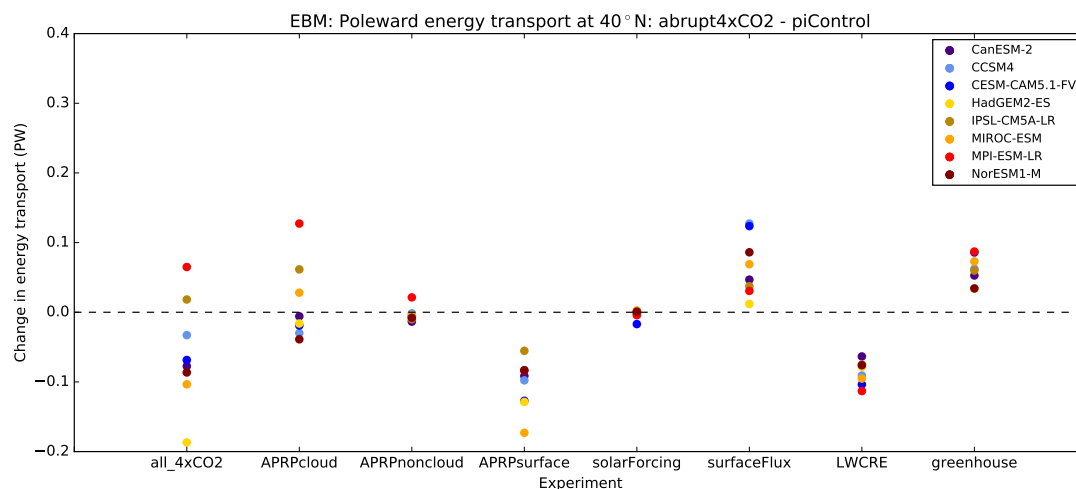
(a)
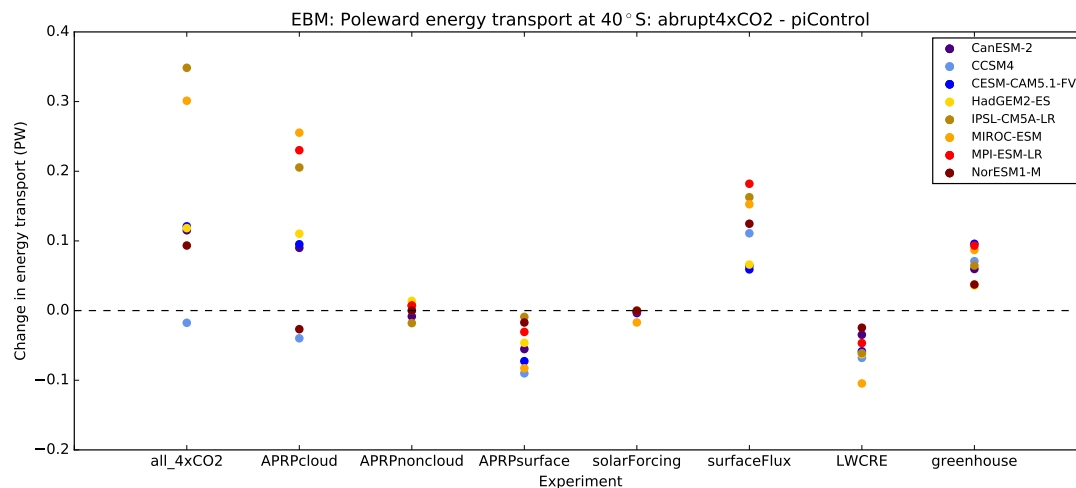
(b)

Figure 8. As in Figure 7 but for abrupt4xCO2 minus piControl.

warming that results in greater poleward energy transport in the full abrupt4xCO2 experiment does not show up when only surface albedo is perturbed.) This feedback term is mainly due to ice melt at high latitudes, which would be expected to reduce the equator-to-pole temperature gradient and therefore also reduce poleward energy transport. The LWCRE experiment also reduces poleward energy transport for abrupt4xCO2, because the LW cloud feedback is positive at high latitudes due to an

5   increase in the optical depth of high clouds (Zelinka et al., 2012). As with G1, non-cloud atmosphere SW feedbacks have small effects on the poleward energy transport for abrupt4xCO2. The solarForcing experiment in this case represents the residual

between the total TOA net shortwave radiation changes and the individual feedback terms calculated using APRP; these effects are minor.

The surfaceFlux experiment has a much greater impact on poleward energy transport for abrupt4xCO2 than for G1, or for the 20th and 21st century CMIP3 runs analyzed by Hwang and Frierson (2010). This is because, while the TOA was kept approximately in energy balance in G1, and the imbalance is relatively small in 20th and 21st century runs, the abrupt4xCO2 case represents a response to an impulse that throws the climate system far out of equilibrium, with much energy being stored in the oceans over time. The abrupt4xCO2 surfaceFlux experiment results in an increase in poleward atmospheric energy transport, which compensates for the energy lost to the ocean at high latitudes.

The all_4xCO2 EBM experiment shows a reduction in poleward energy transport for some models, especially at 40° N, whereas there is an increase in every model in the GCM output (See Figures 2a,d and 5c). Therefore, there must be a mechanism for increased poleward MSE transport at high latitudes that is missed or underestimated by the EBM experiments, or a mechanism for decreased transport that is exaggerated by the EBM. Still, it is useful to see here that cloud feedbacks are significant contributors to the uncertainty in the poleward energy transport changes in abrupt4xCO2 as well as G1. The energy storage term contributes much more to this uncertainty in abrupt4xCO2, which is far out of equilibrium, than in G1, where the global mean energy balance at the TOA is approximately maintained.

4   Conclusions

Our analysis of the GeoMIP G1 ensemble shows that, when CO_2 concentrations are increased and the solar constant is reduced to compensate, poleward atmospheric energy transport decreases. This is because of an increase in polar temperatures and decrease in tropical temperatures, or "residual polar amplification", that results from the different spatial patterns of the opposing solar and CO_2 forcings. The polar warming and tropical cooling cause a decrease in both dry static energy transport, which depends on the equator-to-pole temperature gradient, and latent heat transport, which depends on the meridional gradient of saturation vapor pressure. Residual polar amplification cannot be due to increases in poleward energy transport, as might have been thought, because poleward energy transport actually decreases. It cannot be due to local feedbacks such as the ice-albedo feedback because these feedbacks cannot reverse the sign of an initial temperature change. Instead, the spatial distribution of the combined CO_2 and solar forcing causes this pattern of temperature change, while the decrease in poleward energy transport then acts as a negative feedback that limits the polar warming in G1.

The reduction of poleward energy transport helps explain why the difference in temperature change in the poles and the tropics is not nearly as much in G1 as it is in abrupt4xCO2, or in other words, why solar geoengineering in the form of a uniform solar constant reduction manages to eliminate most (but not all) of the polar amplification of CO_2-induced warming. The role of moisture transport is critical here. When CO_2 is increased by itself, poleward latent heat transport increases because of the large increase in moisture in the tropics, and this amplifies polar warming. In the G1 scenario, by contrast, the cooling of the tropics reduces the amount of moisture in the air, lessening the energy transport to the poles. This indicates that tropical moisture content is a very important control on the meridional temperature gradient. Geoengineering schemes have been

designed that, in GCMs, avoid the problem of over-cooling the tropics by preferentially reducing sunlight in high latitudes (Ban-Weiss and Caldeira, 2010; Kravitz et al., 2016). It would be useful to analyze the changes in atmospheric energy transport in these scenarios in order to better understand the role moisture transport would play in attempting to regulate temperatures in various latitudes.

5   Our EBM attribution experiments illustrate the specific forcings and feedbacks responsible for the changes in meridional energy transport in G1. The solar forcing causes a reduction in poleward energy transport in mid-latitudes; the enhanced greenhouse effect only partially counteracts this. Cloud feedbacks are generally the largest contributors to the inter-model spread in both mid-latitude poleward energy transport changes and cross-equatorial energy transport changes, which are a predictor of ITCZ shifts. The large uncertainty in these quantities associated with clouds implies that an improved physical
10 understanding of the changes in clouds in G1 would help our understanding of how regional precipitation and temperature changes would play out under a solar geoengineering scenario. A more in-depth analysis of the cloud changes in the GeoMIP G1 ensemble will be the subject of a future study.

    The finding that poleward atmospheric energy transport decreases in the G1 experiment relative to piControl is relevant for understanding why polar amplification of warming happens under increased CO_2. In warmer climates, the increased poleward
15 energy transport contributes to the amount of polar amplification that occurs, as evidenced by model studies in which surface albedo is held constant (Alexeev et al., 2005; Graversen and Wang, 2009). However, our analysis of G1 shows that increases in poleward atmospheric energy transport are not necessary in order to have a decrease in the equator-to-pole temperature gradient. These results are particularly interesting in the light of the finding by Hwang et al. (2011) that polar amplification is actually negatively correlated with changes in atmospheric energy transport into the polar regions in CMIP3 global warming
20 simulations. Our results reinforce the conclusion of Hwang et al. (2011) that changes in energy transport alone cannot predict changes in the meridional temperature gradient, which is actually governed by the coupling between energy transport and local feedbacks. It is useful to remember as well that radiative forcings are not spatially uniform, and the structure of the CO_2 forcing can affect atmospheric circulations in warming simulations (Merlis, 2015). The spatial structure of radiative forcing is part of the set of processes, including local feedbacks and energy transport by the atmosphere and ocean, that interactively determine
25 the Earth's meridional temperature pattern. Due to the complexity of these interactions, changes in the temperature gradient cannot be quantitatively predicted without a general circulation model. To better understand these interactions, it would be useful to do further analysis to quantify the contributions of different local feedbacks to the amount of polar warming in the G1 experiment.

Appendix A: Details of GCM-derived energy transport calculations

30 Often, when calculating meridional energy transport based on a cumulative integration of energy flux convergence into the column from GCM output, there is a residual energy transport at the north pole, because the models' internal energy conservation involves terms that are not included in the reported fields energy flux fields, or else because the models used slightly different values of physical constants than we used in our diagnostics. For some models (CCSM4, CESM-CAM5.1-FV, GISS-E2-R,

Table 3. Northward energy transport residual error at north pole in different models and runs, to 4 decimal places.

Model	N (piControl) (PW)	N (G1 - piControl) (PW)	N (abrupt4xCO2 - piControl) (PW)
CanESM-2	-0.0531	0.0411	0.0809
CCSM4	0.0162	-0.0025	0.0015
CESM-CAM5.1-FV	0.0172	-0.0138	0.0027
CSIRO-Mk3L-1-2	0.1429	-0.0093	0.0857
GISS-E2-R	0.0135	-0.0002	0.0033
HadGEM2-ES	-0.0270	0.0137	0.0164
IPSL-CM5A-LR	0.0373	-0.0549	0.0027
MIROC-ESM	-1.9135	0.0593	0.0734
MPI-ESM-LR	-0.1174	0.0526	-0.0515
NorESM1	0.0137	-0.00004	0.0027

HadGEM2-ES, MIROC-ESM and NorESM1-M), this error can be reduced or nearly eliminated by adding $L_f P_{\mathrm{snow}}$ to the right side of Equation 1, where L_f is the latent heat of fusion of ice and P_{snow} is the mass flux of snowfall at the surface. This term accounts for the net energy flux into the atmosphere when snow crystals form in the atmosphere and then melt on land or in the ocean. (We also do this for the calculation of moisture transport in Eq. 2.) For the rest of the models, including this term

5 increases the north pole residual, so we omitted it, assuming that this term had been already accounted for inside the latent heat flux output field. Omitting this term in the first set of models as well did not significantly affect our results.

To correct for any remaining energy flux residual, we subtract the following error function E from the northward energy transport profile:

$$E(\phi) = \frac{N}{2}\left(1 + \sin(\phi)\right) \tag{A1}$$

10 where ϕ is the latitude and N is the residual northward energy transport at the north pole. This correction function assumes that each unit area of Earth's surface contributes equally to the error. To demonstrate that the error is small, Table 3 shows the values of N in piControl and the change in N in the other 2 runs relative to piControl. The errors are generally small (< .15 PW), except for MIROC-ESM, but even in this case the difference in the error between the runs is still small (all models have error < .06 PW for G1 minus piControl, or .09 PW for abrupt4xCO2 minus piControl). Once the correction in Eq. (A1)

15 is applied, the energy transport residual should only affect the results (in terms of differences between runs) if the errors are spatially nonuniform and the spatial pattern of the error differs between the runs. Since even the total error differences are small between runs, these residuals should not be a significant source of error in our analysis.

Appendix B: Details of moist EBM calculations

We use the moist energy balance model first used in Hwang and Frierson (2010). Here we describe how the model works, with an emphasis on new changes made for the solar geoengineering experiments.

The core equation of the model, as in other energy balance models (e.g. North, 1975), is a heat diffusion equation:

$$\frac{\partial T_s}{\partial t} = C \left(\text{EI} - \text{OLR} + D \frac{p_s}{g} \frac{\partial^2 \text{MSE}}{\partial x^2} \right) \qquad (B1)$$

where MSE is the moist static energy, T_s is surface temperature, C is an arbitrary surface heat capacity, OLR is the outgoing longwave radiation at the top of the atmosphere, EI ("energy in") is the net surface and TOA energy flux into the atmospheric column excluding OLR, D is a diffusivity coefficient for MSE, p_s is the surface pressure, g is the acceleration due to gravity, and x is sine of latitude (the sine accounts for area weighting). We assume a value of 1.06×10^6 m^2 s^{-1} for D, following Hwang and Frierson (2010), and a flat topography with $g = 9.8$ m s^{-2} and $p_s = 980$ hPa. Numerically, we use a 2nd-order finite difference for the 2nd derivative of MSE with respect to x, and step forward in time with a relative time step of $\frac{dt}{C} = 1 \times 10^{-4}$. The model is considered to have converged when T_s differs by less than .001 K everywhere in the domain between successive time steps.

The moist static energy is calculated according to:

$$\text{MSE} = C_p T_s + L_v q \qquad (B2)$$

where C_p is the heat capacity of air at constant pressure, L_v is the latent heat of vaporization of water, and q is the specific humidity. We calculate q as a function of T_s using Equation 3, assuming a relative humidity of 80%.

The OLR is treated as a linear function of temperature:

$$\text{OLR} = a T_s - b \qquad (B3)$$

where the coefficients a and b are calculated as linear least-squares fits from the monthly surface air temperature and clear-sky OLR output in each of the GCMs over the first 40 years of piControl. To consider the enhanced greenhouse effect in "perturbation" climates (G1 and abrupt4xCO2), we fit new coefficients a' and b' based on the surface temperature and clear-sky OLR output in those experiments. (Hwang and Frierson (2010) state that they only re-fit b' while keeping a the same, but this appears to be stated in error because when we did the "greenhouse" experiments this way, we found virtually no effect on the EBM results, in contrast to their Figure 4.) Table 4 shows the values of a, b, a' and b' we calculated for each of the GCMs.

To run the EBM, we input the a and b coefficients shown in Table 4, and an EI term calculated differently for the different attribution experiments. For the EBM runs representing piControl conditions, we combine the following terms from the zonal mean output of each GCM:

$$\text{EI}_{\text{piControl}} = S - L_C + F_s \qquad (B4)$$

where S is the net downward SW radiation at the TOA, L_C is the LW cloud radiative effect (clear-sky OLR minus all-sky OLR), and F_s is the net upward surface flux, including SW and LW radiation, sensible heat flux and latent heat flux.

Atmospheric
Chemistry
and Physics
Discussions

Table 4. Values of fit coefficients for clear-sky OLR as a function of temperature for use in moist EBM analysis.

Model	a (W m^{-2} K^{-1})	a' (G1)	a' (abrupt4xCO2)	b (W m^{-2})	b' (G1)	b' (abrupt4xCO2)
CanESM-2	2.0667	1.9934	2.0139	326.83	314.74	320.04
CCSM4	2.1604	2.0898	2.0946	350.06	338.74	341.84
CESM-CAM5.1-FV	2.0724	1.9907	1.9837	328.98	315.19	316.62
HadGEM2-ES	2.1531	2.0942	2.1200	349.37	341.00	349.61
IPSL-CM5A-LR	2.2149	2.1429	2.1504	363.39	350.70	352.36
MIROC-ESM	2.0512	1.9585	1.9732	327.40	310.59	313.99
MPI-ESM-LR	2.0157	1.9284	1.9314	315.55	300.22	300.50
NorESM1	2.1403	2.0665	2.1043	346.36	333.94	344.57

For the "full" perturbation runs emulating the G1 and abrupt4xCO2 experiments, we use a' and b' instead of a and b for the OLR calculation, and the EI term is:

$$\mathrm{EI}_{\mathrm{perturb}} = \mathrm{EI}_{\mathrm{piControl}} + C_S + A_s + I + \Delta L_C + O + \Delta S \tag{B5}$$

where C_S, A_s and I are the change in the net downward TOA SW radiation associated with cloud, non-cloud atmosphere,
5   and surface albedo feedbacks, respectively, calculated using the Approximate Partial Radiation Perturbation (APRP) method
(Taylor et al., 2007); ΔL_C is the change in the LW cloud radiative effect in the GCM output; O is the change in the net surface
flux in the GCM output; and ΔS is the change in the solar forcing. We calculate ΔS by taking the change in net TOA SW
radiation between the control and perturbation climates, and subtracting C_S, A_s, and I to get the change in solar radiation that
is not due to any of the three feedback terms. In G1 this represents the effect of changing the solar constant; in abrupt4xCO2
10   this represents a residual feedback not accounted for by a linear sum of the other 3 feedbacks.

For the individual attribution experiments (except "greenhouse"), we use a and b in the OLR calculation, and the EI terms
are calculated as follows (experiment labels following Table 2):

$$\mathrm{EI}_{\mathrm{APRPcloud}} = \mathrm{EI}_{\mathrm{piControl}} + C_S \tag{B6}$$

$$\mathrm{EI}_{\mathrm{APRPnoncloud}} = \mathrm{EI}_{\mathrm{piControl}} + A_s \tag{B7}$$

15   $$\mathrm{EI}_{\mathrm{APRPsurface}} = \mathrm{EI}_{\mathrm{piControl}} + I \tag{B8}$$

$$\mathrm{EI}_{\mathrm{solarForcing}} = \mathrm{EI}_{\mathrm{piControl}} + \Delta S \tag{B9}$$

$$\mathrm{EI}_{\mathrm{surfaceFlux}} = \mathrm{EI}_{\mathrm{piControl}} + O \tag{B10}$$

$$\mathrm{EI}_{\mathrm{LWCRE}} = \mathrm{EI}_{\mathrm{piControl}} + \Delta L_C \tag{B11}$$

For the "greenhouse" experiment, we use the control value of EI, but use a' and b' instead of a and b for the OLR calculation.

The northward energy transport output by the EBM and shown in figures 6 through 8 is the cumulative meridional integration of the MSE diffusion term in Eq. (B1). The discretization of the diffusion equation for numerical solving inevitably results in some loss of energy, so after integrating, we apply a correction for residual northward transport at the North Pole for the EBM results, using Eq. (A1).

5 *Author contributions.* R.D. Russotto analyzed the GCM output, ran the EBM attribution experiments, produced the figures, and wrote the bulk of the paper. T.P. Ackerman provided general guidance and assisted with the preparation of the manuscript text.

Code availability All scripts used to analyze data and create plots are available here: atmos.washington.edu/articles/GeoMIP_EnergyTransport_PolarAmplification_ITCZ. A standalone Python code for the APRP method is available at: https://github.com/rdrussotto/pyAPRP.

Atmospheric
Chemistry
and Physics
Discussions

References

Alexeev, V. A., Langen, P. L., and Bates, J. R.: Polar amplification of surface warming on an aquaplanet in "ghost forcing" experiments without sea ice feedbacks, Climate Dynamics, 24, 655–666, doi:10.1007/s00382-005-0018-3, http://dx.doi.org/10.1007/s00382-005-0018-3, 2005.

5 Arora, V. K., Scinocca, J. F., Boer, G. J., Christian, J. R., Denman, K. L., Flato, G. M., Kharin, V. V., Lee, W. G., and Merryfield, W. J.: Carbon emission limits required to satisfy future representative concentration pathways of greenhouse gases, Geophysical Research Letters, 38, L05805, doi:10.1029/2010GL046270, 2011.

Ban-Weiss, G. and Caldeira, K.: Geoengineering as an optimization problem, Environmental Research Letters, 5, 034009, doi:10.1088/1748-9326/5/3/034009, 2010.

10 Bekryaev, R. V., Polyakov, I. V., and Alexeev, V. A.: Role of Polar Amplification in Long-Term Surface Air Temperature Variations and Modern Arctic Warming, Journal of Climate, 23, 3888–3906, doi:10.1175/2010JCLI3297.1, 2010.

Bentsen, M., Bethke, I., Debernard, J. B., Iversen, T., Kirkevåg, A., Seland, Ø., Drange, H., Roelandt, C., Seierstad, I. A., Hoose, C., and Kristjánsson, J. E.: The Norwegian Earth System Model, NorESM1-M – Part 1: Description and basic evaluation of the physical climate, Geoscientific Model Development, 6, 687–720, doi:10.5194/gmd-6-687-2013, 2013.

15 Broccoli, A. J., Dahl, K. A., and Stouffer, R. J.: Response of the ITCZ to Northern Hemisphere cooling, Geophysical Research Letters, 33, L01702, doi:10.1029/2005GL024546, 2006.

Chiang, J. C. H. and Bitz, C. M.: Influence of high latitude ice cover on the marine Intertropical Convergence Zone, Climate Dynamics, 25, 477–496, doi:10.1007/s00382-005-0040-5, 2005.

Collins, W. J., Bellouin, N., Doutriaux-Boucher, M., Gedney, N., Halloran, P., Hinton, T., Hughes, J., Jones, C. D., Joshi, M., Liddicoat, S.,
20 Martin, G., O'Connor, F., Rae, J., Senior, C., Sitch, S., Totterdell, I., Wiltshire, A., and Woodward, S.: Development and evaluation of an Earth-System model – HadGEM2, Geoscientific Model Development, 4, 1051–1075, doi:10.5194/gmd-4-1051-2011, 2011.

Dufresne, J.-L., Foujols, M.-A., Denvil, S., Caubel, A., Marti, O., Aumont, O., Balkanski, Y., Bekki, S., Bellenger, H., Benshila, R., Bony, S., Bopp, L., Braconnot, P., Brockmann, P., Cadule, P., Cheruy, F., Codron, F., Cozic, A., Cugnet, D., de Noblet, N., Duvel, J.-P., Ethé, C., Fairhead, L., Fichefet, T., Flavoni, S., Friedlingstein, P., Grandpeix, J.-Y., Guez, L., Guilyardi, E., Hauglustaine, D., Hourdin, F., Idelkadi,
25 A., Ghattas, J., Joussaume, S., Kageyama, M., Krinner, G., Labetoulle, S., Lahellec, A., Lefebvre, M.-P., Lefevre, F., Levy, C., Li, Z. X., Lloyd, J., Lott, F., Madec, G., Mancip, M., Marchand, M., Masson, S., Meurdesoif, Y., Mignot, J., Musat, I., Parouty, S., Polcher, J., Rio, C., Schulz, M., Swingedouw, D., Szopa, S., Talandier, C., Terray, P., Viovy, N., and Vuichard, N.: Climate change projections using the IPSL-CM5 Earth System Model: from CMIP3 to CMIP5, Climate Dynamics, 40, 2123–2165, doi:10.1007/s00382-012-1636-1, 2013.

Ferraro, A. J. and Griffiths, H. G.: Quantifying the temperature-independent effect of stratospheric aerosol geoengineering on global-mean
30 precipitation in a multi-model ensemble, Environmental Research Letters, 11, 034012, doi:10.1088/1748-9326/11/3/034012, 2016.

Frierson, D. M. W. and Hwang, Y.-T.: Extratropical Influence on ITCZ Shifts in Slab Ocean Simulations of Global Warming, Journal of Climate, 25, 720–733, doi:10.1175/JCLI-D-11-00116.1, 2012.

Gent, P. R., Danabasoglu, G., Donner, L. J., Holland, M. M., Hunke, E. C., Jayne, S. R., Lawrence, D. M., Neale, R. B., Rasch, P. J., Vertenstein, M., Worley, P. H., Yang, Z.-L., and Zhang, M.: The Community Climate System Model Version 4, Journal of Climate, 24,
35 4973–4991, doi:10.1175/2011JCLI4083.1, 2011.

Giorgetta, M. A., Jungclaus, J., Reick, C. H., Legutke, S., Bader, J., Böttinger, M., Brovkin, V., Crueger, T., Esch, M., Fieg, K., Glushak, K., Gayler, V., Haak, H., Hollweg, H.-D., Ilyina, T., Kinne, S., Kornblueh, L., Matei, D., Mauritsen, T., Mikolajewicz, U., Mueller, W.,

Atmospheric
Chemistry
and Physics
Discussions

Open Access

Notz, D., Pithan, F., Raddatz, T., Rast, S., Redler, R., Roeckner, E., Schmidt, H., Schnur, R., Segschneider, J., Six, K. D., Stockhause, M., Timmreck, C., Wegner, J., Widmann, H., Wieners, K.-H., Claussen, M., Marotzke, J., and Stevens, B.: Climate and carbon cycle changes from 1850 to 2100 in MPI-ESM simulations for the Coupled Model Intercomparison Project phase 5, Journal of Advances in Modeling Earth Systems, 5, 572–597, doi:10.1002/jame.20038, 2013.

5 Govindasamy, B. and Caldeira, K.: Geoengineering Earth's radiation balance to mitigate CO2-induced climate change, Geophysical Research Letters, 27, 2141–2144, doi:10.1029/1999GL006086, http://dx.doi.org/10.1029/1999GL006086, 2000.

Govindasamy, B., Caldeira, K., and Duffy, P.: Geoengineering Earth's radiation balance to mitigate climate change from a quadrupling of CO2, Global and Planetary Change, 37, 157 – 168, doi:http://dx.doi.org/10.1016/S0921-8181(02)00195-9, http://www.sciencedirect.com/science/article/pii/S0921818102001959, evaluation, Intercomparison and Application of Global Climate Models, 2003.

10 Graversen, R. G. and Wang, M.: Polar amplification in a coupled climate model with locked albedo, Climate Dynamics, 33, 629–643, doi:10.1007/s00382-009-0535-6, http://dx.doi.org/10.1007/s00382-009-0535-6, 2009.

Hartmann, D. L.: Global Physical Climatology, Elsevier, Amsterdam, Netherlands, 2nd edn., 2016.

Haywood, J. M., Jones, A., Bellouin, N., and Stephenson, D.: Asymmetric forcing from stratospheric aerosols impacts Sahelian rainfall, Nature Climate Change, 3, 660–665, doi:10.1038/NCLIMATE1857, 2013.

15 Haywood, J. M., Jones, A., Dunstone, N., Milton, S., Vellinga, M., Bodas-Salcedo, A., Hawcroft, M., Kravitz, B., Cole, J., Watanabe, S., and Stephens, G.: The impact of equilibrating hemispheric albedos on tropical performance in the HadGEM2-ES coupled climate model, Geophysical Research Letters, 43, 395–403, doi:10.1002/2015GL066903, http://dx.doi.org/10.1002/2015GL066903, 2015GL066903, 2016.

Held, I. M. and Soden, B. J.: Robust Responses of the Hydrological Cycle to Global Warming, Journal of Climate, 19, 5686–5699, doi:http://dx.doi.org/10.1175/JCLI3990.1, 2006.

20 Holland, M. M. and Bitz, C. M.: Polar amplification of climate change in coupled models, Climate Dynamics, 21, 221–232, doi:10.1007/s00382-003-0332-6, 2003.

Hurrell, J. W., Holland, M. M., Gent, P. R., Ghan, S., Kay, J. E., Kushner, P. J., Lamarque, J.-F., Large, W. G., Lawrence, D., Lindsay, K., Lipscomb, W. H., Long, M. C., Mahowald, N., Marsh, D. R., Neale, R. B., Rasch, P., Vavrus, S., Vertenstein, M., Bader, D., Collins, W. D., Hack, J. J., Kiehl, J., and Marshall, S.: The Community Earth System Model: A Framework for Collaborative Research, Bulletin of the
25 American Meteorological Society, 94, 1339–1360, doi:10.1175/BAMS-D-12-00121.1, 2013.

Hwang, Y.-T. and Frierson, D. M. W.: Increasing atmospheric poleward energy transport with global warming, Geophysical Research Letters, 37, L24807, doi:10.1029/2010GL045440, 2010.

Hwang, Y.-T., Frierson, D. M. W., and Kay, J. E.: Coupling between Arctic feedbacks and changes in poleward energy transport, Geophysical Research Letters, 38, L17704, doi:10.1029/2011GL048546, 2011.

30 Hwang, Y.-T., Frierson, D. M. W., and Kang, S. M.: Anthropogenic sulfate aerosol and the southward shift of tropical precipitation in the late 20th century, Geophysical Research Letters, 40, 2845–2850, doi:10.1002/grl.50502, 2013.

Kravitz, B., Robock, A., Boucher, O., Schmidt, H., Taylor, K. E., Stenchikov, G., and Schulz, M.: The Geoengineering Model Intercomparison Project (GeoMIP), Atmospheric Science Letters, 12, 162–167, doi:10.1002/asl.316, 2011.

Kravitz, B., Caldeira, K., Boucher, O., Robock, A., Rasch, P. J., Alterskjær, K., Karam, D. B., Cole, J. N. S., Curry, C. L., Haywood, J. M.,
35 Irvine, P. J., Ji, D., Jones, A., Kristjánsson, J. E., Lunt, D. J., Moore, J. C., Niemeier, U., Schmidt, H., Schulz, M., Singh, B., Tilmes, S., Watanabe, S., Yang, S., and Yoon, J.-H.: Climate model response from the Geoengineering Model Intercomparison Project (GeoMIP), Journal of Geophysical Research: Atmospheres, 118, 8320–8332, doi:10.1002/jgrd.50646, 2013a.

Kravitz, B., Rasch, P. J., Forster, P. M., Andrews, T., Cole, J. N. S., Irvine, P. J., Ji, D., Kristjánsson, J. E., Moore, J. C., Muri, H., Niemeier, U., Robock, A., Singh, B., Tilmes, S., Watanabe, S., and Yoon, J.-H.: An energetic perspective on hydrological cycle changes in the Geoengineering Model Intercomparison Project, Journal of Geophysical Research: Atmospheres, 118, 13,087–13,102, doi:10.1002/2013JD020502, 2013b.

5 Kravitz, B., MacMartin, D., Wang, H., and Rasch, P.: Geoengineering as a design problem, Earth System Dynamics, 7, 469–497, doi:10.5194/esd-7-469-2016, 2016.

Merlis, T. M.: Direct weakening of tropical circulations from masked CO_2 radiative forcing, Proceedings of the National Academy of Sciences, 112, 13 167–13 171, doi:10.1073/pnas.1508268112, http://www.pnas.org/content/112/43/13167.abstract, 2015.

Niemeier, U., Schmidt, H., Alterskjær, K., and Kristjánsson, J. E.: Solar irradiance reduction via climate engineering: Impact of differ-
10 ent techniques on the energy balance and the hydrological cycle, Journal of Geophysical Research: Atmospheres, 118, 11,905–11,917, doi:10.1002/2013JD020445, 2013.

North, G. R.: Theory of Energy-Balance Climate Models, Journal of the Atmospheric Sciences, 32, 2033–2043, 1975.

Pendergrass, A. G. and Hartmann, D. L.: The Atmospheric Energy Constraint on Global-Mean Precipitaton Change, Journal of Climate, 27, 757–768, 2014.

15 Phipps, S. J., Rotstayn, L. D., Gordon, H. B., Roberts, J. L., Hirst, A. C., and Budd, W. F.: The CSIRO Mk3L climate system model version 1.0 – Part 1: Description and evaluation, Geoscientific Model Development, 4, 483–509, doi:10.5194/gmd-4-483-2011, 2011.

Pithan, F. and Mauritsen, T.: Arctic amplification dominated by temperature feedbacks in contemporary climate models, Nature Geoscience, 7, 181–184, doi:10.1038/ngeo2071, 2014.

Schmidt, G. A., Kelley, M., Nazarenko, L., Ruedy, R., Russell, G. L., Aleinov, I., Bauer, M., Bauer, S. E., Bhat, M. K., Bleck, R., Canuto,
20 V., Chen, Y.-H., Cheng, Y., Clune, T. L., Del Genio, A., de Fainchtein, R., Faluvegi, G., Hansen, J. E., Healy, R. J., Kiang, N. Y., Koch, D., Lacis, A. A., LeGrande, A. N., Lerner, J., Lo, K. K., Matthews, E. E., Menon, S., Miller, R. L., Oinas, V., Oloso, A. O., Perlwitz, J. P., Puma, M. J., Putman, W. M., Rind, D., Romanou, A., Sato, M., Shindell, D. T., Sun, S., Syed, R. A., Tausnev, N., Tsigaridis, K., Unger, N., Voulgarakis, A., Yao, M.-S., and Zhang, J.: Configuration and assessment of the GISS ModelE2 contributions to the CMIP5 archive, Journal of Advances in Modeling Earth Systems, 6, 141–184, doi:10.1002/2013MS000265, 2014.

25 Smyth, J. E., Russotto, R. D., and Storelvmo, T.: Thermodynamic and dynamic responses of the hydrological cycle to solar dimming, Atmospheric Chemistry and Physics, pp. 1–17, doi:10.5194/acp-2016-886, http://www.atmos-chem-phys-discuss.net/acp-2016-886/, accepted article, 2017.

Swann, A. L. S., Fung, I. Y., and Chiang, J. C. H.: Mid-latitude afforestation shifts general circulation and tropical precipitation, Proceedings of the National Academy of Sciences, 109, 712–716, doi:10.1073/pnas.1116706108, 2012.

30 Taylor, K. E., Crucifix, M., Braconnot, P., Hewitt, C. D., Doutriaux, C., Broccoli, A. J., Mitchell, J. F. B., and Webb, M. J.: Estimating Shortwave Radiative Forcing and Response in Climate Models, Journal of Climate, 20, 2530–2543, doi:10.1175/JCLI4143.1, 2007.

Tilmes, S., Fasullo, J., Lamarque, J.-F., Marsh, D. R., Mills, M., Alterskjær, K., Muri, H., Kristjánsson, J. E., Boucher, O., Schulz, M., Cole, J. N. S., Curry, C. L., Jones, A., Haywood, J., Irvine, P. J., Ji, D., Moore, J. C., Karam, D. B., Kravitz, B., Rasch, P. J., Singh, B., Yoon, J.-H., Niemeier, U., Schmidt, H., Robock, A., Yang, S., and Watanabe, S.: The hydrological impact of geoengineering in the Geoengineering
35 Model Intercomparison Project (GeoMIP), Journal of Geophysical Research: Atmospheres, 118, 11,036–11,058, doi:10.1002/jgrd.50868, 2013.

Watanabe, S., Hajima, T., Sudo, K., Nagashima, T., Takemura, T., Okajima, H., Nozawa, T., Kawase, H., Abe, M., Yokohata, T., Ise, T., Sato, H., Kato, E., Takata, K., Emori, S., and Kawamiya, M.: MIROC-ESM 2010: model description and basic results of CMIP5-20C3M experiments, Geoscientific Model Development, 4, 845–872, doi:10.5194/gmd-4-845-2011, 2011.

Zelinka, M. D., Klein, S. A., and Hartmann, D. L.: Computing and Partitioning Cloud Feedbacks Using Cloud Property Histograms. Part II:

5   Attribution to Changes in Cloud Amount, Altitude, and Optical Depth, J. Climate, 25, 3736–3754, doi:http://dx.doi.org/10.1175/JCLI-D-11-00249.1, 2012.